Anisotropic Locally-Conformal Perfectly Matched Layer for Higher Order Curvilinear Finite-Element Modeling

Aaron P. Smull, *Student Member, IEEE,* Ana B. Manić, *Member, IEEE*, Sanja B. Manić, *Student Member, IEEE*, and Branislav M. Notaroš, *Fellow, IEEE*

Abstract—**A perfectly matched layer (PML) method is proposed for electrically large curvilinear meshes based on a higher order finite-element modeling paradigm and the concept of transformation electromagnetics. The method maps the non-Maxwellian formulation of the locally-conformal PML to a purely Maxwellian implementation using continuously varying anisotropic and inhomogeneous material parameters. An approach to implementation of a conformal PML for higher order meshes is also presented, based on a method of normal projection for PML mesh generation around an already existing convex volume mesh of a dielectric scatterer, with automatically generated constitutive material parameters. Once the initial mesh is generated, a PML optimization method based on gradient descent is implemented to most accurately match the PML material parameters to the geometrical interface. The numerical results show that the implementation of a conformal PML in the higher order finite-element modeling paradigm dramatically reduces the reflection error when compared to traditional PMLs with piecewise constant material parameters. The ability of the new PML to accurately and efficiently model scatterers with a large variation in geometrical shape and those with complex material compositions is demonstrated in examples of a dielectric almond and a continuously inhomogeneous and anisotropic transformation-optics cloaking structure, respectively.**

Index Terms—**Numerical algorithms, computational electromagnetics, finite element method, perfectly matched layer, transformation electromagnetics, scattering, higher order modeling, polynomial basis functions, curved parametric elements, hexahedral elements, numerical optimization.**

I. INTRODUCTION

Boundary conditions in open-domain problems have long been an issue in computational electromagnetics (CEM) in the use of partial differential equation (PDE) based methods such as the finite element method (FEM) or the finite difference time domain method (FDTD) [1]. When dealing with electromagnetic radiation or scattering problems, effective truncation of the computational domain is a well-investigated problem both in the frequency-domain and the time-domain. Various methods such as operator-based absorbing boundary conditions (ABCs) [2-3] and hybrid boundary element method/FEM formulations [4-5] have been employed to mimic the behavior of an unbounded space in a bounded computational domain. Without carefully chosen boundary conditions, truncation of an otherwise infinite domain leads to artificial wave reflections.

The perfectly matched layer (PML) serves as a practical and effective alternative to traditional ABCs – instead of applying a specially formulated and generally difficult to implement boundary condition, an artificial lossy domain is added around the computational domain. This additional domain serves as a numerical analogue to pyramidal absorbers in an anechoic chamber. Incident fields propagate without reflection into the artificial domain and are attenuated before reaching the true edge of the computational domain, ensuring any numerical reflections from domain truncation do not contribute to the overall solution. The original perfectly matched layer was born as an alternative method to traditional ABC's in the context of the FDTD method by Berenger [6]. The method utilized a splitting of the fields in Cartesian coordinates to derive a lossy material exhibiting the desired behavior. Alternatively, Chew and Weedon formulated an alternate derivation of the PML, originating from the idea of complex-coordinate stretching [7]. The coordinates of the original wave equation are effectively stretched from Euclidean space $\mathbb{R}^3$ onto a complex-valued manifold $\mathbb{C}^3$. With a redefinition of the curl operator in complex space, the outward propagating fields can be matched to exponentially decaying fields in the PML domain. Sacks et al. showed in [8] that the PML could alternatively be formulated in Cartesian coordinates as a set of anisotropic absorbers. These anisotropic elements are derived based on matching boundary conditions at the interface of air and a lossy material, and act identically to the complex coordinate stretching based method.

Pendry and Ward promoted the field of transformation optics/electromagnetics in their landmark paper [9], showing that the form of Maxwell's equations in the frequency domain can be preserved under a change of coordinates if the constitutive material parameters are altered accordingly. Following this line of work, the coordinate stretching

formulation and anisotropic formulation can be seen as alternate formulations of an identical principle. The concept of complex coordinate based transformation was further extended to provide anisotropic PMLs in a variety of canonical geometries including spherical and cylindrical systems [10] and to match less usual material parameters including bianisotropic and lossy dispersive media [11-12].

Utilizing a local orthogonal coordinate system generated from Darboux frames, the perfectly matched layer was eventually extended by Teixeira and Chew to conform to general orthogonal coordinate systems [13]. Conformal PMLs have a distinct computational advantage over any fixed implementation, because the convex hull of a given scatterer or antenna is in general not spherical or rectangular. In order to match such geometry to one of the fixed PML implementations, requires the use of additional computational whitespace via unnecessary air elements. The rectangular PML has the benefit that, if the stretching function is linear, the material parameters in the anisotropic PML domain will be piecewise constant [8]. Such a benefit is not inherited by other PML boundary shapes, such as the cylindrical or spherical implementations.

In [14], the locally-conformal PML for FEM was introduced, which forgoes solutions of Maxwell's equations for direct solutions of the modified set of equations, on a redefined complex manifold. Unlike the method based on local orthogonal coordinate systems, this PML formulation by Ozgun and Kuzuoglu requires no explicit dependence on the principle radii of curvature. As such, this method extends the complex stretching introduced to a larger class of geometries, simply by replacing the position element nodes with their complex-valued counterparts. In general, such formulations are referred to as non-Maxwellian, because the equations of interest are not the original Maxwell's equations, but the modified form using the redefined curl operator.

More recently, a variety of other conformal PML implementations for FEM modeling have subsequently appeared in literature involving the application to finite-element time-domain (FETD) techniques. Most notably, a scheme for implementation of the PML in the mixed FETD context was presented in [15], which allows the simultaneous calculation of scattering over a wide band of frequencies. Alternatively, a separate method was presented in the context of discontinuous Galerkin (DG) FEM [16]. These methods again cast the PML as a set of anisotropic material functions derived from local orthogonal coordinate frames.

Continuing to use the concept derived from the field of transformation electromagnetics [17], here we map the non-Maxwellian formulation of the locally-conformal PML to a purely Maxwellian implementation using continuously varying anisotropic and inhomogeneous material parameters. We propose a novel PML method for use with electrically large curvilinear meshes based on a higher order FEM modeling paradigm and the concept of transformation electromagnetics. The interpolatory parameterization of higher order curvilinear geometries provides an interface to evaluate the required Jacobian matrices in a simple and effective manner. To the best of our knowledge, there has not been a significant work in the development of a conformal PML method for large, arbitrarily shaped, curved, higher order finite elements. This is the first higher order anisotropic locally-conformal PML-FEM method.

In addition, while the theoretical continuation of the PML to arbitrary element sizes and shapes follows from much of the past work on PMLs, many details of relevance to the implementation of such a method are entirely non-trivial in practice. PML implementation utilizing higher order modeling presents a unique set of challenges and advantages when compared to its low-order counterpart. One of these challenges is the automatic creation of a perfectly matched layer and the numerical calculation of the proper constitutive material parameters. It is well known that the majority of reflection error from perfectly matched layers is due to the associated discretization errors – as the name implies, the reflection would theoretically be zero in the case of infinite discretization accuracy [18]. One should expect that continuously inhomogeneous material approximations and curved PML interfaces should show significant performance improvement over the standard low-order modeling paradigm. In particular, we believe that the method of normal projection for generation of a conformal PML for higher order meshes and gradient-descent based PML material optimization algorithm described in Section III are very significant to this body of work. The basic theory and preliminary results of the new anisotropic locally-conformal PML for a higher-order curvilinear FEM are presented in a summary form in [19-20].

With recent advances in photonics and material sciences, and with the advent of manufacturing and design of metamaterial-based structures, we believe it is of a significant interest within the CEM community for the continual development of scattering codes to ease in the theoretical design phase of devices based on such metamaterials. There is an active push for commercialized design of metamaterial components [21]. Microscopic subwavelength features used in metamaterial design are too small to be modeled or to be resolved by an electromagnetic wave, but often admit bulk properties as effective anisotropic materials. Spatial variations in micro- and nanofabrication can lead to materials with effectively continuously inhomogeneous permittivity and permeability tensors. The future of electromagnetic and optical design will involve the computer-aided realization of metamaterial devices. This includes the accurate theoretical open-region modeling of electromagnetic devices containing arbitrary inhomogeneous and anisotropic media.

The rest of the paper is organized as follows. Section II outlines the exact finite element formulation, including the scattered-field wave formulation, parametrized curvilinear geometrical discretization, the set of hierarchical curl-conforming higher order vector basis functions, and continuously varying inhomogeneous and anisotropic material parameters for accurate modeling of arbitrary linear materials. Section III describes in detail the development of the perfectly matched layer scheme, beginning with the complex coordinate transformation leading to the PML behavior. It also presents a

novel approach to implementation of a conformal PML for higher order meshes; namely, by using a method of normal projection, the meshing of a PML around an already existing convex volume mesh can be done in a largely hands off manner. Once the initial mesh has been generated, a PML optimization method based on gradient descent is implemented to most effectively match the free-space impedance to the material parameters of the PML. In Section IV, several numerical examples are presented for numerical validation and comparison of the proposed method with alternate modeling paradigms. In particular, we examine the discretization error from finite element approximations regarding piecewise anisotropic material parameters, and compare these to the higher order material approximations provided by this method. We continue by investigating the effect of PML parameters on the discretization error. We then model a dielectric almond to show the behavior of the conformal perfectly matched layer on more diverse geometries. Finally, we examine a continuously inhomogeneous cloaking structure based on transformation optics.

II. Finite Element Formulation

Higher order polynomials as basis functions are well known for the increase in the approximation accuracy of electric field solutions in the FEM [22]. The standard for mesh discretization in low-order modeling is usually taken to have elements no larger than $\lambda/10$ in each dimension, λ being the wavelength in the medium. With the use of higher order basis functions and curved parametric elements, one is able to do large-domain modeling, with elements sized up to 2λ.

Electromagnetic scattering can be analyzed in the frequency domain by dividing the electric field into incident and scattered components and writing the double-curl vector wave equation [18],

$$\nabla \times \overline{\overline{\mu}}_r^{-1} \nabla \times \mathbf{E}^{sc} - k_0^2 \overline{\overline{\varepsilon}}_r \mathbf{E}^{sc} =$$
$$-\nabla \times \overline{\overline{\mu}}_r^{-1} \nabla \times \mathbf{E}^{inc} + k_0^2 \overline{\overline{\varepsilon}}_r \mathbf{E}^{inc} \qquad (1)$$

Since the incident field must be a solution to Maxwell's equations in free space, we may subtract the free-space contribution from the incident side of equation (1) to arrive at a scattering formulation for finite element implementation,

$$\nabla \times \overline{\overline{\mu}}_r^{-1} \nabla \times \mathbf{E}^{sc} - k_0^2 \overline{\overline{\varepsilon}}_r \mathbf{E}^{sc} =$$
$$-\nabla \times (\overline{\overline{\mu}}_r^{-1} - \overline{\overline{I}}) \nabla \times \mathbf{E}^{inc} + k_0^2 (\overline{\overline{\varepsilon}}_r - \overline{\overline{I}}) \mathbf{E}^{inc} \qquad (2)$$

After testing equation (2) via the Galerkin procedure, and making use of appropriate boundary conditions, the finite element formulation of (2) can be written as (assuming that the entire computational domain is surrounded by a perfect electrically conducting boundary)

$$\int (\nabla \times \mathbf{f}) \cdot \overline{\overline{\mu}}_r^{-1} (\nabla \times \mathbf{E}^{sc}) dV - k_0^2 \int \mathbf{f} \cdot \overline{\overline{\varepsilon}}_r \mathbf{E}^{sc} \, dV$$

$$= -\int (\nabla \times \mathbf{f}) \cdot \overline{\overline{\mu}}_r^{-1} (\nabla \times \mathbf{E}^{inc}) dV + k_0^2 \int \mathbf{f} \cdot \overline{\overline{\varepsilon}}_r \mathbf{E}^{inc} \, dV \qquad (3)$$

The geometrical discretization of the scattering body is given by generalized curvilinear hexahedrons of arbitrary order defined by a set of Lagrange interpolatory polynomials. These can be described in terms of a mapping from a local set of coordinates (u, v, w) to their position by [22]

$$\mathbf{r}(u,v,w) = \sum_{k=0}^{K_u} \sum_{l=0}^{K_v} \sum_{m=0}^{K_w} \mathbf{r}_{klm} L_k^{K_u}(u) L_l^{K_v}(v) L_m^{K_w}(w), \qquad (4a)$$

where K_u, K_v, and K_w are a set of geometric orders, $L_i(x)$ is the ith Lagrange interpolatory polynomial for a set of $K_i + 1$ equally spaced interpolation points. The local parametric coordinates are constrained to the unit cube,

$$-1 \leq u, v, w \leq 1 \qquad (4b)$$

For computational efficiency, a change of basis is undergone in order to describe the mapping (equivalently) in the polynomial basis of the local coordinates as

$$\mathbf{r}(u,v,w) = \sum_{k=0}^{K_u} \sum_{l=0}^{K_v} \sum_{m=0}^{K_w} \hat{\mathbf{r}}_{klm} u^k v^l w^m. \qquad (4c)$$

This basis change allows for quick computational determination of intermediate element points during integration, as well as providing a simpler form for the evaluation of necessary derivatives during the implementation of the PML layer.

The scattered electric field vector over each element is approximated by a set of hierarchical curl-conforming polynomial vector basis functions as follows:

$$\mathbf{E}^{sc} = \sum_{i=0}^{N_u-1} \sum_{j=0}^{N_v} \sum_{k=0}^{N_w} \alpha_{ijk}^{(u)} \mathbf{f}_{ijk}^{(u)} + \sum_{i=0}^{N_u} \sum_{j=0}^{N_v-1} \sum_{k=0}^{N_w} \alpha_{ijk}^{(v)} \mathbf{f}_{ijk}^{(v)}$$
$$+ \sum_{i=0}^{N_u} \sum_{j=0}^{N_v} \sum_{k=0}^{N_w-1} \alpha_{ijk}^{(w)} \mathbf{f}_{ijk}^{(w)}, \qquad (5)$$

where the polynomial vector basis is defined as, for example,

$$\mathbf{f}_{ijk}^{(u)}(u,v,w) = u^i \hat{P}_j(v) \hat{P}_k(w) \mathbf{a}^u \qquad (6a)$$

$$\hat{P}_i(x) = \begin{cases} 1-x, & i=0 \\ 1+x, & i=1 \\ P_i(x) - P_{i-2}(x), & i \geq 2 \end{cases} \qquad (6b)$$

Here, P_i denotes the ith order Legendre polynomial [23]. These basis functions are defined in terms of a set of contravariant (dual) basis vectors ($\mathbf{a}^u$, $\mathbf{a}^v$, $\mathbf{a}^w$) determined by the local parametric coordinates (u, v, w) of each element. The dual basis vectors are given in terms of the covariant basis vectors ($\mathbf{a}_u$, $\mathbf{a}_v$, $\mathbf{a}_w$) and the Jacobian of the local-to-global coordinate transform as:

$$\mathbf{a}^{u} = \frac{\mathbf{a}_v \times \mathbf{a}_w}{|\mathbf{J}|}, \mathbf{a}^{v} = \frac{\mathbf{a}_w \times \mathbf{a}_u}{|\mathbf{J}|}, \mathbf{a}^{w} = \frac{\mathbf{a}_u \times \mathbf{a}_v}{|\mathbf{J}|} \qquad (7)$$

$$|\mathbf{J}| = \mathbf{a}_w \cdot (\mathbf{a}_u \times \mathbf{a}_v) \qquad (8)$$

$$\mathbf{a}_u = \frac{d\mathbf{r}}{du}, \mathbf{a}_v = \frac{d\mathbf{r}}{dv}, \mathbf{a}_w = \frac{d\mathbf{r}}{dw} \qquad (9)$$

The higher order modeling paradigm offers a few degrees of flexibility over traditional finite element methods. One of these is the ability to model general anisotropic and continuously varying material parameters [24]. This is accomplished by a similar Lagrange interpolation scheme to (4). For a general anisotropic, inhomogeneous material, we expand the continuously inhomogeneous material tensors in terms of the material tensors at the interpolation points as

$$\bar{\bar{\varepsilon}}_r(u,v,w) = \sum_{k=0}^{K'_u} \sum_{l=0}^{K'_v} \sum_{m=0}^{K'_w} \bar{\bar{\varepsilon}}_{r,klm} L_k^{K'_u}(u) L_l^{K'_v}(v) L_m^{K'_w}(w), \qquad (10)$$

and similarly for $\bar{\bar{\mu}}_r$. Note that the material approximation orders $K'_{u/v/w}$ may generally be chosen independently of the geometrical approximation order $K_{u/v/w}$.

III. CONFORMAL PERFECTLY MATCHED LAYER

This conformal PML implementation is generated via a spatial transformation based upon the locally-conformal formulation of the stretched-coordinate PML introduced by Ozgun and Kuzuoglu [14]. The PML consists of a layer of artificial anisotropic media. The goal is to generate an anisotropic PML layer around the existing mesh. We assume that a convex mesh of a scattering body exists, including a surrounding air cushion layer.

The first step of the PML implementation is to generate a geometrical model of the conformal PML layer given a higher order mesh. This can be accomplished via a method of projections. At each geometrical node on the surface, the unit normal to the surface is calculated. The surface normal directions are simply the dual basis vectors given by (7). The normal on nodes shared by multiple elements (corners and
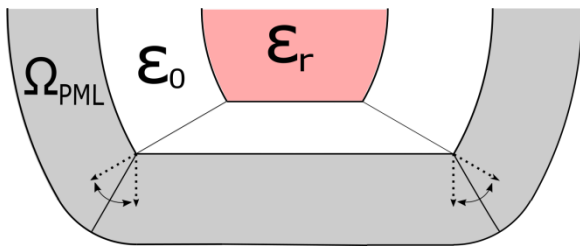
element edges) are averaged to determine the direction of projection. After the projection direction has been calculated for each node, elements constituting the PML layer are generated by projecting outwards along these directions by a predetermined PML thickness. Because the higher order modeling paradigm allows for electrically large elements, only a single element is needed for projection from each element face. A visualization of this process is given in Fig. 1.

The locally-conformal PML is initially defined by a complex coordinate transform which effectively "stretches" the coordinates in the PML away from the real domain boundary into a complex space. This is accomplished by introducing a coordinate transformation inside the PML as [14]

$$\tilde{\mathbf{r}} = \mathbf{r} - \frac{j}{k_0} f_1(\|\mathbf{r} - \mathbf{r}_0\|) \frac{(\mathbf{r} - \mathbf{r}_0)}{\|\mathbf{r} - \mathbf{r}_0\|} + \frac{1}{k_0} f_2(\|\mathbf{r} - \mathbf{r}_0\|) \frac{(\mathbf{r} - \mathbf{r}_0)}{\|\mathbf{r} - \mathbf{r}_0\|} \qquad (11)$$

Each material interpolation point inside the generated PML layer is mapped back to the closest point on the surface of the previous computational domain. A given point in the PML domain P with position $\mathbf{r}$ is "stretched" (in a complex manner) away from the closest point on the PML P_0, with position $\mathbf{r}_0$ defined by

$$\mathbf{r}_0 = \min_{\mathbf{r} \in \partial\Omega_{pml}} \|\mathbf{r} - \mathbf{r}_0\| \qquad (12)$$

The imaginary complex factor serves the purpose of mapping oscillating fields to decaying ones. Additionally, by introducing a real coordinate stretching factor, the PML additionally serves the purpose of attenuating evanescent fields faster within the artificial layer.

This PML formulation allows the implementation of particularly troublesome areas where the radii of curvature on the initial mesh may be 0 and methods based on local orthogonal coordinate systems may fail [14]. Figure 2 shows

Fig. 1: An illustration of the projection process applied to an arbitrarily shaped curved geometrically higher order mesh. Starting from the dielectric scatterer and surrounding air layer, the normal to the element face is calculated at each node on the mesh surface. An element is generated by projecting outwards along this normal. At corner regions, the surface normals are averaged to produce a direction of projection.
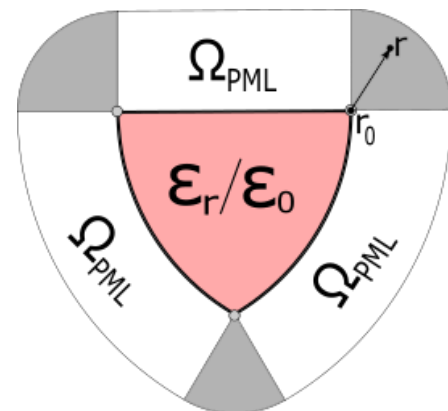

Fig. 2: Visualization in 2 dimensions of a conformal PML layer around a predefined geometry (including a dielectric scatterer and air cushion). The shaded areas in the PML layer correspond to corner regions, in which the principle curvatures diverge, and the complex stretching function throughout the region maps back to the corner point $\mathbf{r}_0$. The closest point on the PML boundary everywhere in this region is the corner point. Each point in these shaded areas will be effectively stretched away from these corner points.

what these traditionally troublesome regions look like. In regions generated from corners, the entire PML region may simply be stretched away from the corner points.

The requirement on the stretching functions $f_i(\|\mathbf{r}-\mathbf{r}_0\|)$ is that they be monotonically increasing functions of the distance from the PML boundary. For example, these can be polynomial functions given by

$$f_1(\|\mathbf{r}-\mathbf{r}_0\|) = \alpha_1\|\mathbf{r}-\mathbf{r}_0\|^p, \; f_2(\|\mathbf{r}-\mathbf{r}_0\|) = \alpha_2\|\mathbf{r}-\mathbf{r}_0\|^p, \quad (13)$$

where p is a positive exponent. For simplicity, we consider $p = 1$ in our implementation. Note that $p = 3, 4$ are the typical choices to minimize spurious reflection from the PML in the FDTD context. Our future study will address the optimal choice of p in the higher order FEM context.

After every material interpolation point in the PML domain has been mapped to its according complex coordinate via (6), we can again define a Lagrange-based interpolation in the polynomial basis of (u, v, w) as:

$$\tilde{\mathbf{r}}(u,v,w) = \sum_{k=0}^{K_u}\sum_{l=0}^{K_v}\sum_{m=0}^{K_w}\hat{\tilde{\mathbf{r}}}_{klm}u^k v^l w^m. \quad (14)$$

Maxwell's equations are well known to be invariant under coordinate transformations. Maxwell's equations on a modified coordinate system have the same formal appearance as the original Maxwell's equations with alternate material parameters. By modifying the permittivity and permeability tensors,

$$\bar{\bar{\varepsilon}}_r{}' = \frac{\tilde{\mathbf{J}}^T\bar{\bar{\varepsilon}}_r\tilde{\mathbf{J}}}{|\tilde{\mathbf{J}}|}, \qquad \bar{\bar{\mu}}_r{}' = \frac{\tilde{\mathbf{J}}^T\bar{\bar{\mu}}_r\tilde{\mathbf{J}}}{|\tilde{\mathbf{J}}|} \qquad (15a)$$

$$\tilde{\mathbf{J}} = \frac{\partial\mathbf{x}}{\partial\tilde{\mathbf{x}}} = \begin{bmatrix} \dfrac{\partial x}{\partial\tilde{x}} & \dfrac{\partial x}{\partial\tilde{y}} & \dfrac{\partial x}{\partial\tilde{z}} \\[2mm] \dfrac{\partial y}{\partial\tilde{x}} & \dfrac{\partial y}{\partial\tilde{y}} & \dfrac{\partial y}{\partial\tilde{z}} \\[2mm] \dfrac{\partial z}{\partial\tilde{x}} & \dfrac{\partial y}{\partial\tilde{y}} & \dfrac{\partial y}{\partial\tilde{z}} \end{bmatrix} \qquad (15b)$$

we can obtain the same behavior of the fields as if the complex coordinate transformation (11) were implemented. Such an idea forms the basis for an entire body of work in transformation optics/electromagnetics theory [9,17].

The interpolative mapping admits the Jacobian of the complex coordinate transform to be written in terms of the Jacobians of a given elements coordinate interpolation (1) and complex coordinate interpolation (9). By the chain rule, this Jacobian is given by

$$\tilde{\mathbf{J}} = \tilde{\mathbf{J}}_{elem}^{-1}\mathbf{J}_{elem} \qquad (16a)$$

$$\mathbf{J}_{elem} = \frac{\partial\mathbf{x}}{\partial\mathbf{u}}, \tilde{\mathbf{J}}_{elem} = \frac{\partial\tilde{\mathbf{x}}}{\partial\mathbf{u}}. \qquad (16b)$$

Equations (15) and (16) together define the anisotropic material parameters given a complex coordinate transformation.

The minimization problem given by (12) has a unique solution provided the starting mesh is convex [10], which is already a necessary condition for the attenuating behavior of the perfectly matched layer [25]. While the projection process gives us an approximate idea of the closest point on a given mesh surface, it is not always exact. Failure to satisfy the condition given by (12) leads to an imperfectly matched boundary and numerical reflections.

To overcome this difficulty, it is useful to implement a numerical optimization algorithm to overcome any errors imposed by the projection process. For a given point, using its point of projection as a starting point, a search over the adjacent element faces is performed to ensure satisfaction of the condition in (12). We evaluate the aforementioned minimization problem numerically by means of a constrained gradient descent algorithm [26]. The gradient descent is evaluated to map back to the surface of the element from which it was projected, as well as the immediately surrounding elements on the surface.

The gradient descent algorithm involves starting with an initial guess on the PML boundary for the position of the point $\mathbf{r}_0$, and continually updating the guess based on the partial derivatives of a given cost function. The cost function to be minimized is the square of the distance between the interpolation point $\mathbf{r}$ and surface point $\mathbf{r}_0$,

$$f_c(u,v,w) = \|\mathbf{r}-\mathbf{r}_0(u,v,w)\|^2 \qquad (17)$$

The algorithm begins with a guess equal to the point of projection, and continually updates the (u,v,w) coordinates of the guess, based on the gradient of (17) as

$$(u,v,w)_{k+1} = (u,v,w)_k - \beta\nabla f_c(u,v,w)\gamma^k \qquad (18a)$$

$$\nabla f_c(u,v,w) = \left(\frac{\partial f_c}{\partial u}, \frac{\partial f_c}{\partial v}, \frac{\partial f_c}{\partial w}\right) \qquad (18b)$$

The factor β is a constant, which is dependent upon the absolute scale of the problem, and the factor γ^k is included to ensure convergence of the algorithm in the case of oscillations around a local minimum. The update is continually constrained to stay within the unit cube (4b), and terminates if the update in position is below a selected tolerance. The derivatives associated with the gradient in (18) are easily calculated from the interpolatory definition of the element (4c).

After the calculation of new effective material parameters based on the gradient descent algorithm (18) and the appropriate material transformation (15), the matrices of interest are filled as usual by the Galerkin procedure via the integrals in (3). The incident field is set to be a plane wave (or other exciting field of interest) in the physical domain, but is

not present in the PML region. The right-hand side only needs to be filled for elements which are not part of the PML.

IV. NUMERICAL RESULTS

All simulations were run using Colorado State Universty's ISTeC Cray High Performance Computing (HPC) System. The Cray HPC System is a Model XE6 computing system with 32 compute cores per node, and utilizes a Gemini 3D-torus interconnect [27]. Distributed direct solutions of the associated sparse system of equations were found using multifrontal-based LU factorizations via the MUMPS library [28].

For our first numerical example, we analyze the difference in accuracy between piecewise constant and continuously inhomogeneous material parameters in the anisotropic perfectly matched layer. The perfectly matched layer derives from a set of exact impedance matching conditions which theoretically yields zero reflected waves. However, discretization errors lead to spurious reflections, which we wish to minimize. One should expect an increase in the accuracy of the PML in the higher order modeling paradigm, in which material parameters are described by continuous interpolatory polynomials. The well-known example of the sphere admits an analytical solution in the form of Mie's series [18], which can be used to quantify the error of a given PML discretization.

This example utilizes 15,317 2nd order curved geometrical elements to mesh a small dielectric sphere with relative permittivity $\varepsilon_r = 2.25$. The radius of the sphere is 0.5 m at 300 MHz, with a 0.3-m thick air cushion, a 0.3-m thick PML layer, and a field approximation order $N_u = N_v = N_w = 3$. The total number of unknowns involved in such a discretization, which satisfies that no edge length is greater than $\lambda/10$, is 1,225,260. The use of 3rd order field approximation makes this example very over-refined, in order to isolate the error caused by the material parameter approximation from geometrical modeling errors and errors caused from a lack of mesh refinement.

This model is run with automatically generated material approximation parameters, and again with a piecewise approximation to the appropriate material parameters. A comparison of the numerical errors in the bistatic radar cross section (RCS) in the two cases is shown in Fig. 3. It is shown that by using a continuous approximation to the required material parameters, the reflection error is decreased by 1 to 2 orders of magnitude.

The second numerical example helps to illustrate the effect of the PML parameters on the numerical error in a setting based on practical discretization error. One of the advantages of a higher-order modeling paradigm for the PML is to reduce the complexity of modeling the PML by generating it from a single element projected outwards. For this reason, it is of interest to compare a practical modeling scheme where the PML is instead modeled by a single layer. We consider a dielectric spherical scatterer example identical to the first example, with variation in the parameters of the PML. The dielectric sphere is well overrefined, as is the $0.3\lambda_0$ thick spherical air cushion surrounding it, with λ_0 denoting the wavelength in air (free space). Rather than overrefining the
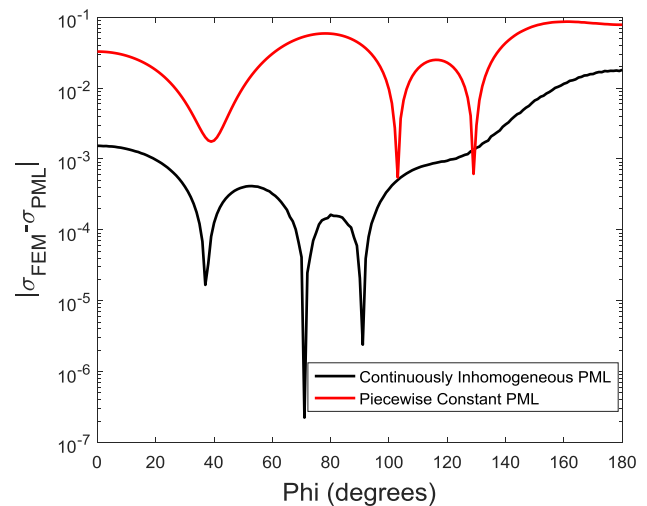

Fig. 3: Error in bistatic radar cross section of a 1λ diameter homogeneous dielectric sphere of relative permittivity $\varepsilon_r = 2.25$. The sphere is excited by a plane wave incident from the $\phi = 0$ direction. A factor of 10 improvement in the numerical error is seen by using a continuously inhomogeneous PML when compared to piecewise constant material parameters.

PML, we investigate the effects of element size. The mesh is made spherically symmetric with well overrefined elements in the transverse directions, but with more modest discretization in the radial direction. For practical purposes, the PML layer is meshed with a single radial layer of elements, with $N = 3$ field expansion, 2nd order geometry, and 2nd order material interpolation. This represents a very reasonable and practical modeling paradigm for higher-order finite elements. We vary both the thickness of the PML layer, t_{PML}, as well as the coefficient α_1 of the linear stretching function, in (13). Within a range of parameters around our most common choice, it is found that the discretization error has a fairly drastic dependence on the PML stretching parameter as well as the thickness of the PML layer. The RMS error in the normalized bistatic RCS is calculated for a sweep of these parameters and is presented in Table I.

At low values of α_1/k_0 (k_0 is the free-space wave number), the model converges slowly with increasing the t_{PML}, because of the exponential decay of the outgoing waves. At high values of α_1/k_0, the model becomes extremely sensitive to the PML thickness because the exponentially decaying waves are

TABLE I. RMS error in bistatic radar cross section (dB) of the dielectric scatterer from Fig. 3 for a sweep of the PML parameters, the thickness of the PML layer, t_{PML}, and the coefficient α_1 of the linear stretching function.

		t_{PML}/λ_0						
		.1	.15	.2	.25	.3	.35	.4
α_1/k_0	1.33	8.377	5.642	3.952	3.634	1.885	1.074	1.014
	1.67	7.089	4.129	2.676	2.081	1.295	0.905	1.020
	2.00	5.897	2.029	1.726	1.609	0.714	0.851	1.253
	2.33	4.844	2.200	1.080	0.574	0.653	1.164	1.947
	2.67	3.945	1.556	0.614	0.348	0.991	1.606	2.206
	3.00	3.193	1.340	0.676	0.105	1.406	2.076	2.733

TABLE II. RMS error (e_{RMS}) in bistatic RCS (dB) of the dielectric scatterer from Fig. 3 for different values of the air layer thickness, t_{air}.

t_{air}/λ_0	.1	.15	.2	.25	.3	.35	.4
e_{RMS}	1.482	1.579	1.344	0.835	0.799	0.987	1.386

not well approximated by the space of basis functions. We find that the minimum error is obtained for $\alpha_1 = 3.0k_0$ and $t_{PML} = 0.25\lambda_0$. However, at these values, the solution is somewhat sensitive to variations in these parameters. At higher values of α_1, the fields decay faster than the solution can accurately model, and the error again increases. In practice, we settle for a more moderate nominal selection of $\alpha_1 = 2.5k_0$ and $t_{PML} = 0.3\lambda_0$. We find that this represents a decent balance between the accuracy of the solution and the sensitivity of the accuracy with respect to the PML parameters. Next, we fix the values of these parameters at $\alpha_1 = 2.5k_0$ and $t_{PML} = 0.3\lambda_0$ and investigate the effect of the thickness of the air layer, t_{air}, on the same error function. We keep the air layer well overrefined (maximum element size $< 0.1\lambda_0$). The results are shown in Table II. Overall, only a minimal effect is seen on the error, and especially around the value of $t_{air} = 0.3\lambda_0$. We hereafter adopt $t_{air} = 0.3\lambda_0$ in all examples.

The third numerical example examines the ability of the in conformal PML on a more complicated geometry. The NASA almond model geometry [29] is used as a dielectric scatterer with $\varepsilon_r = 2.25$. The almond shape serves as a useful benchmark for CEM methods, because the round back and sharp tip provide a variation in geometrical shape. The excitation is by a vertically polarized plane wave incident on the tip of the almond (from the −x direction). The starting mesh consisted solely of the dielectric almond, and the projection procedure described in Section III was repeated twice to generate a $0.3\lambda_0$ air layer and a $0.3\lambda_0$ PML layer. The entire mesh including the air and PML consisted of 928 2nd order geometric elements.

Figure 4 shows a comparison of the near scattered electric field of the dielectric almond in the FEM discretization with
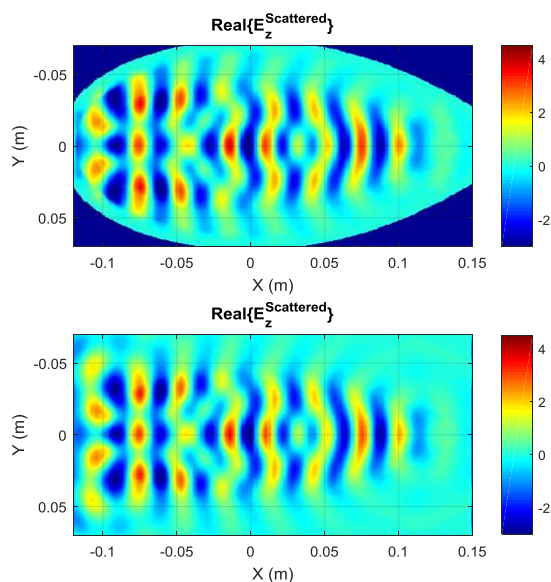
conformal PML with that obtained using a method of moments (MoM) solution from the industry solver WIPL-D [30]. An excellent agreement of the two sets of results is observed.

Figure 5 shows the comparison of the bistatic RCS of the almond. Good agreement is observed in the far-field pattern as well. Because of the tapered shape of the almond, one would expect the presence of evanescent fields, particularly at the scattering tip, due to the possible occurrence of total internal reflection inside the dielectric. To account for this, a real coordinate stretching function f_2 of the form given in eq. (11) is included with $\alpha_2 = 0.8k_0$. Indeed, we found that such an implementation was necessary to provide agreement with the MoM solution in the far-field.

The fourth and final numerical example is a simulation of a spherical continuously inhomogeneous and anisotropic
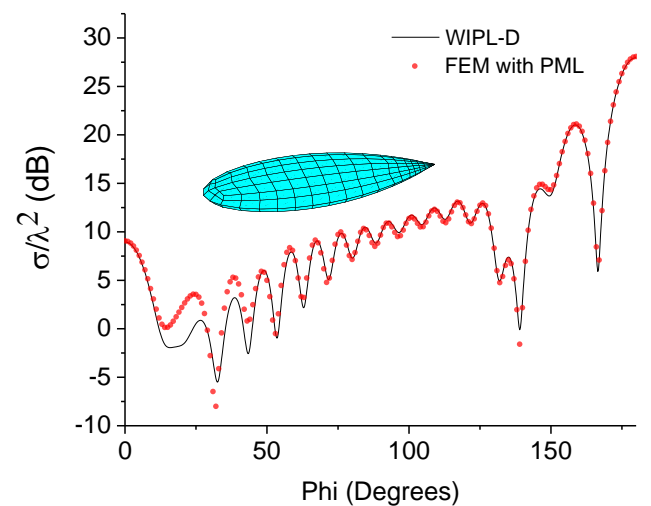
Fig. 5: Normalized bistatic cross section of a dielectric almond scatterer with relative permitivitty $\varepsilon_r = 2.25$. The incident field is a *z*-polarized plane wave of frequency 10 GHz from the −x direction. The cross-section is validated with the use of WIPL-D, a surface integral equation solver.

cloaking structure. Such a structure can be described in terms of theory from transformation optics [31]. In [32], a higher order spherical cloak was simulated using continuously inhomogeneous material parameters based on a FEM-MoM hybrid formulation to deal with boundary conditions. We simulate a dielectric sphere with diameter of 3λ and a relative permittivity of $\varepsilon_r = 2.25$. The cloak is based on a linear mapping function, and consists entirely of an inhomogeneous layer 2 elements thick. The material parameters from [31] are approximated by 4th order interpolations. The entire sphere and cloaking structure is surrounded by a $0.3\lambda_0$ layer of air and a $0.3\lambda_0$ thick PML. Figure 6 shows the normalized bistatic RCS calculated from the entire device, compared to the Mie's series solution. We see a reduction of the cross section to less than 50 dB around the entirety of the sphere. Figure 7 shows a snapshot in time of the z-directed electric field in and around the dielectric sphere. The incident waves are in essence bent around the sphere, and the electric field inside the dielectric is reduced to near zero.

Fig. 4: (top) Real part of the near scattered electric field (*z*-component) of the dielectric almond, as calculated by the FEM with conformal PML. Plane wave is incident from the +x direction and is *z*-polarized. (bottom) The same near scattered field based on MoM surface integral equation calculations via WIPL-D. Note the wave attenuation in the immediately surrounding region (the PML) in the FEM solution.
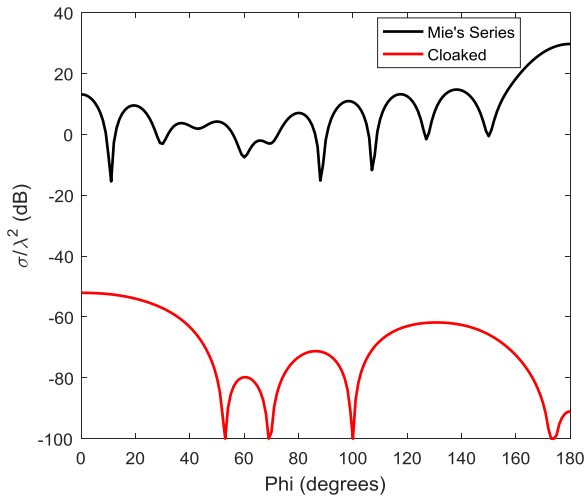
Fig. 6: Normalized bistatic cross section of a continuously inhomogeneous and anisotropic cloaking structure consisting of a dielectric sphere of diameter 3λ and relative permittivity $\varepsilon_r = 2.25$ with a 2 elements thick cloak layer based on a linear mapping function,

V. Conclusions

This paper has proposed a novel perfectly matched layer method for use with electrically large curvilinear meshes based on a higher order FEM modeling paradigm and the concept of transformation electromagnetics. The method maps the non-Maxwellian formulation of the locally-conformal PML to a purely Maxwellian implementation using continuously varying anisotropic and inhomogeneous material parameters, with the interpolatory parameterization of higher order curvilinear geometries providing an interface to evaluate the required Jacobian matrices in a simple and effective manner. The paper has also presented a novel approach to implementation of a conformal PML for higher order meshes, based on a method of normal projection for PML mesh generation around an already existing convex volume mesh of a dielectric scatterer, with automatically generated constitutive material parameters. Starting with such an initially generated mesh, a PML optimization method based on gradient descent is used to most effectively match the free-space impedance to the material parameters of the PML. Overall, this appears to be the first higher order anisotropic locally-conformal PML-FEM method.

The numerical results have shown that the implementation of a conformal perfectly matched layer in the higher order FEM modeling paradigm provides benefits over traditional PMLs with piecewise constant material parameters, with the reflection error in a spherical dielectric scatterer example being reduced by a factor of 10 to 100 using the higher order material approximations inherent to the new method. The ability of the new anisotropic locally-conformal higher order PML to accurately and efficiently analyze scatterers with a large variation in geometrical shape has been demonstrated in an example of a dielectric almond, which is challenging for PML modeling because of the sharp tip and round back, as well as the tapered shape of the almond. The performance of the method in analysis of objects with unconventional and challenging to model material compositions has been

demonstrated in an example of a spherical continuously inhomogeneous and anisotropic cloaking structure based on transformation optics.

While the novel PML method can be applied to FEM modeling, analysis, and design of arbitrary structures, one of the areas of practical application and our future work is its utilization to aid in the theoretical design and analysis of novel devices based on metamaterials.
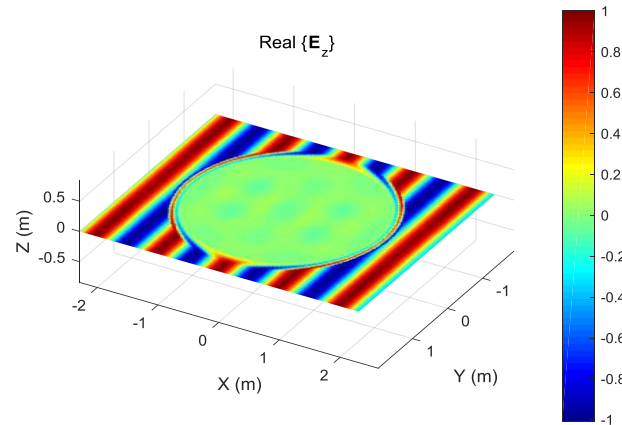

Fig. 7: A snapshot of the total electric field (z-component) in the near-field of an electromagnetic cloaking device. The exotic material parameters surrounding a dielectric sphere effectively bend an incident plane wave around the scattering body. The plane wave propagation exhibits only minimal disturbance by the presence of the entire structure.

References

[1] K. S. Kunz and R.J. Luebbers. *The finite difference time domain method for electromagnetics*. CRC press, 1993

[2] J. P. Webb and V. N. Kanellopoulos, "Absorbing boundary conditions for the finite element solution of the vector wave equation," Microwave and Optical Technology Letters, Vol. 2, No. 10, October 1989, pp. 370-372.

[3] A. Chatterjee, J.-M. Jin, and J. L. Volakis, "A finite element formulation with absorbing boundary conditions for three dimensional scattering", IEEE Transactions on Antennas and Propagation, Vol. 41, No. 2, pp. 221-226, February 1993.

[4] X. Yuan, D. R. Lynch, and J. W. Strohbehn. "Coupling of finite element and moment methods for electromagnetic scattering from inhomogeneous objects."

[5] D. J. Hoppe, L.W. Epp, J.-F. Lee, "A hybrid symmetric FEM/MOM formulation applied to scattering by inhomogeneous bodies of revolution", *IEEE Trans. Antennas Propag,* vol. 42, pp. 798-805, 1994.

[6] J. P. Berenger, "A perfectly matched layer for the absorption of electromagnetic waves," *J. Comput. Phys.*, vol. 114, pp. 185-200, Oct. 1994.

[7] W. C. Chew and W. H. Weedon, "A 3D perfectly matched medium from modified Maxwell's equations with stretched coordinates," *Microw. Opt. Technol. Lett.*, vol. 7, pp. 599-604, Sept. 1994.

[8] Z. S. Sacks, D. M. Kingsland, R. Lee, and J.-F. Lee, "A perfectly matched anisotropic absorber for use as an absorbing boundary condition," *IEEE Trans. Antennas Propag.,* vol 43, pp. 1460-1463, Dec. 1995.

[9] A. J. Ward and J. B. Pendry, "Refraction and geometry in Maxwell's equations," J. Modern. Optics, vol. 43, pp. 773-793, 1996.

[10] F. L. Teixeira and W. C. Chew, "Systematic Derivation of Anisotropic PML Absorbing Media in Cylindrical and Spherical Coordinates," *IEEE Microw. Guided Wave. Lett.,* vol. 7, pp. 371-373, Nov. 1997.

[11] S. D. Gedney, "An anisotropic PML absorbing media for the FDTD simulation of fields in lossy and dispersive media," *Electromagn.,* Vol. 16, pp. 399-415, 1996.

[12] F. L. Teixeira and W. C. Chew, "General closed-form PML constitutive tensors to match arbitrary bianisotropic and dispersive linear media,"

IEEE Microwave and Guided Wave Lett., vol. 8, pp. 223-225, June 1998.

[13] F. L. Teixeira and W. C. Chew, "Analytical derivation of a conformal perfectly matched absorber for electromagnetic waves," *Microw. Opt. Technol. Lett.*, vol. 17, pp. 231–236, March 1998.

[14] O. Ozgun and M. Kuzuoglu, "Non-Maxwellian locally-conformal PML absorbers for finite element mesh truncation," *IEEE Trans. Antennas Propag.*, vol. 55, pp. 931-937, March 2007.

[15] B. Donderici and F. L. Teixeira, "Conformal Perfectly Matched Layer for the Mixed Finite Element Time-Domain Method," *IEEE Trans. Antennas Propag.,* vol. 56, pp. 1017-1026, April 2008.

[16] S. Dosopoulos and J.-F. Lee, "Interior Penalty Discontinuous Galerkin Finite Element Method for the Time-Dependent First Order Maxwell's Equations," *IEEE Trans. Antennas Propag.,* vol. 58, December 2010.

[17] D-H. Kwon, D. H. Werner, "Transformation electromagnetics: an overview of the theory and applications" *IEEE Antenn. Propag. Mag.*, vol. 52, pp. 24–46, 2010.

[18] J.-M. Jin, *Theory and computation of electromagnetic fields*. John Wiley & Sons, 2011.

[19] A. P. Smull, A. B. Manić, S. B. Manić, and B. M. Notaroš, "Double Higher-Order FEM Modeling Using An Anisotropic Conformal Perfectly Matched Layer," *Proc. of the 2016 IEEE International Symposium on Antennas and Propagation*, Fajardo, Puerto Rico, pp. 1119–1120, June 26–July 1, 2016.

[20] A. P. Smull, A. B. Manić, S. B. Manić, and B. M. Notaroš, "Double-Higher-Order Finite Element Modeling of a Conformal Perfectly Matched Layer for Electromagnetic Scattering Simulation," *Proc. 2016 USNC-URSI National Radio Science Meeting*, Boulder, Colorado, January 6-9, 2016.

[21] A. Alù, "Metamaterials: Prime time." *Nature Materials,* vol. 15, pp. 1229-1231, Nov. 2016.

[22] M. M. Ilić and B. M. Notaroš, "Higher order hierarchical curved hexahedral vector finite elements for electromagnetic modeling," *IEEE Trans. Microw. Theory Tech.*, vol. 51, pp. 1026–1033, Mar. 2003.

[23] M. M. Ilić and B. M. Notaroš, "Higher order large-domain hierarchical FEM technique for electromagnetic modeling using Legendre basis functions on generalized hexahedra," *Electromagnetics*, vol. 26, pp. 517–529, Oct. 2006.

[24] A. B. Manić, S. B. Manić, M. M. Ilić, and B. M. Notaroš, "Large anisotropic inhomogeneous higher order hierarchical generalized hexahedral finite elements for 3-D electromagnetic modeling of scattering and waveguide structures." *Microw. Opt. Technol. Lett.*, vol. 54, pp. 1644-1649, July 2012.

[25] K. Sainath and F. L. Teixeira. "Perfectly reflectionless omnidirectional absorbers and electromagnetic horizons." *JOSA B,* vol. 32, pp. 1645-1650, 2015.

[26] E. K. Chong and S. H. Zak. *An introduction to optimization*. John Wiley & Sons, 2013.

[27] istec.colostate.edu/activities/hpc/cray, *ISTeC Cray High Performance Computing System*

[28] http://mumps.enseeiht.fr, *MUMPS Users Guide*.

[29] A. C. Woo, H. T. G. Wang, M. J. Schuh, and M. L. Sanders, "Benchmark radar targets for the validation of computational electromagnetic programs," *IEEE Antennas Propagat. Mag.*, Vol. 35, pp. 84–89, Feb. 1993.

[30] www.wipl-d.com, *WIPL-D*

[31] J. B. Pendry, D. Schurig, D. R. Smith, "Controlling Electromagnetic Fields." *Science,* vol. 312, pp. 1780-1782, 2006.

[32] S. V. Savić, A. B. Manić, M. M. Ilić, B. M. Notaroš, "Efficient Higher Order Full-Wave Numerical Analysis of 3-D Cloaking Structures", *Plasmonics,* pp. 455-463, 2013.

Aaron P. Smull (S'15) was born in Santa Rosa, California in 1993. He received his B.S. (2015) and M.S. (2017) in Electrical Engineering from Colorado State University, and is currently pursuing his PhD in physics and the University of California, Berkeley. His current research interests include the development of numerical algorithms for the classical and quantum interaction of electromagnetic waves with matter, and the development of novel quantum information processing technologies through the study of atomic physics.

Ana B. Manić was born in Belgrade, Serbia, in 1986. She graduated with B.S. from the Department of Electronics in the School of Electrical Engineering at Belgrade University in 2009. She received her Ph.D. degree at Colorado State University, Department of Electrical and Computer Engineering, in 2015. During her Ph.D. study, she worked on different applications of the method of moments in computational electromagnetics such as: method of moments coupling with the finite element method, diakoptics domain decomposition method, fast direct solvers, accurate and efficient calculation of singular and hypersingular integrals arising in the Galerkin-type method of moments system of equations, etc.

Sanja B. Manić was born in Belgrade, Serbia, in 1986. She received the B.S. degree in 2010 from the Department of Electronics, School of Electrical Engineering, Belgrade University, Serbia. She is a Ph.D. student, since 2010, at the Department of Electrical and Computer Engineering, Colorado State University. Her interests are in computational electromagnetics, higher order surface integral equation method of moments, higher order finite element method, iterative solvers and weather precipitation modeling.

Branislav M. Notaroš (M'00-SM'03-F'16) received the Dipl.Ing. (B.S.), M.S., and Ph.D. degrees in electrical engineering from the University of Belgrade, Belgrade, Yugoslavia, in 1988, 1992, and 1995, respectively.

From 1996 to 1999, he was an Assistant Professor in the School of Electrical Engineering at the University of Belgrade. He spent the 1998-1999 academic year as a Visiting Scholar at the University of Colorado at Boulder. He was an Assistant Professor, from 1999 to 2004, and Associate Professor, from 2004 to 2006, in the Department of Electrical and Computer Engineering at the University of Massachusetts Dartmouth. From 2006 to 2012, he was an Associate Professor in the Department of Electrical and Computer Engineering at Colorado State University, where he is currently a Professor and University Distinguished Teaching Scholar, as well as Director of Electromagnetics Laboratory. His research interests and activities are in computational electromagnetics, higher order numerical methods, antennas, scattering, microwaves, metamaterials, characterization of snow and rain,

surface and radar precipitation measurements, RF design for MRI at ultra-high magnetic fields, and electromagnetics education. His publications include more than 200 journal and conference papers, and three workbooks in electromagnetics and in fundamentals of electrical engineering (basic circuits and fields). He is the author of textbooks *Electromagnetics* (Prentice Hall, 2010), *MATLAB-Based Electromagnetics* (Prentice Hall, 2013), and *Conceptual Electromagnetics* (CRC Press, 2017).

Dr. Notaroš is Fellow of the IEEE and of the Applied Computational Electromagnetics Society (ACES). He served as General Chair for the 11th International Workshop on Finite Elements for Microwave Engineering – FEM2012, June 4-6, 2012, Estes Park, Colorado, USA, and as Guest Editor of the Special Issue on Finite Elements for Microwave Engineering, Electromagnetics, Vol. 34, Issue 3-4, 2014. He serves as General Chair of the 2018 International Applied Computational Electromagnetics Society Symposium – ACES2018, March 24-29, 2018, Denver, Colorado, USA, and of the 14th International Workshop on Finite Elements for Microwave Engineering – FEM2018, September 10-14, 2018, Cartagena de las Indias, Colombia. He is Associate Editor for the IEEE Transactions on Antennas and Propagation. He serves on the Board of Directors of ACES, as ACES Secretary, and as Chair of the Technical Committee for the Commission B of the US National Committee, International Union of Radio Science (URSI). He was the recipient of the 2005 IEEE MTT-S Microwave Prize (best-paper award for IEEE Transactions on MTT), 1999 IEE Marconi Premium (best-paper award for IEE Proceedings on Microwaves, Antennas and Propagation), 1999 URSI Young Scientist Award, 2005 UMass Dartmouth Scholar of the Year Award, 2004 UMass Dartmouth College of Engineering Dean's Recognition Award, 1992 Belgrade Chamber of Industry and Commerce Best M.S. Thesis Award, 2009, 2010, 2011, and 2014 Colorado State University Electrical and Computer Engineering Excellence in Teaching Awards, 2010 Colorado State University College of Engineering George T. Abell Outstanding Teaching and Service Faculty Award, 2012 Colorado State University System Board of Governors Excellence in Undergraduate Teaching Award, 2014 Colorado State University Provost's N. Preston Davis Award for Instructional Innovation, 2012 IEEE Region 5 Outstanding Engineering Educator Award, 2014 Carnegie Foundation for the Advancement of Teaching Colorado Professor of the Year Award, 2015 American Society for Engineering Education ECE Distinguished Educator Award, and 2015 IEEE Undergraduate Teaching Award.